

Influence of the Metallic Load of Pt/C and Pt_{0.6}-Ru_{0.4}/C Nanowires on the Electrochemical Oxidation of Methanol in Acid Medium

Gláucia R.O. Almeida^{1,2}, Eliana M. Sussuchi³, Cristiano T. de Meneses⁴,
Giancarlo R. Salazar-Banda^{1,2}, Katlin I.B. Eguiluz^{1,2,*}

¹ Programa de Pós-Graduação em Engenharia de Processos, Universidade Tiradentes, 49032–490, Aracaju, SE, Brasil.

² Laboratório de Eletroquímica e Nanotecnologia, Instituto de Tecnologia e Pesquisa (ITP), 49032–490, Aracaju, SE, Brasil

³ Departamento de Química, Universidade Federal de Sergipe, 49100-000, São Cristóvão, SE, Brasil.

⁴ Departamento de Física, Universidade Federal de Sergipe, 49506-036, Itabaiana, SE, Brasil.

*E-mail: katlinbarrios@gmail.com

Received: 4 April 2017 / Accepted: 3 June 2017 / Published: 12 July 2017

This work aimed on the development of platinum and platinum-ruthenium nanowires supported on carbon powder, via chemical reduction using formic acid as a reducing agent, and the study of electrooxidation of methanol in acidic medium on these catalysts. The metal load of the nanowires in relation to the substrate was varied from 20, 30 and 40% and their composition for the Pt–Ru/C nanowires was maintained at 60:40. The nanocatalysts were characterized by X-ray diffraction, X-ray fluorescence, transmission electron microscopy (TEM) and cyclic voltammetry, showing that the nanowires have the cubic face-centered structure of platinum. The chemical composition of the catalysts is close to nominal. The TEM images showed that Pt/C and Pt_{0.6}Ru_{0.4}/C nanowires were successfully synthesized by the chemical reduction method presenting nanowires with a diameter between 4 and 13 nm and a length between 15 and 20 nm. The Pt_{0.6}Ru_{0.4}/C 20% catalytic composite exhibit the lowest CO oxidation onset potential (0.34 V) which is 0.3 V more negative than the obtained for a commercial Pt/C catalyst. The current density of the CO-stripping peak at the Pt_{0.6}Ru_{0.4}/C 20% catalytic composite is also 3 times higher than for the commercial Pt/C. The incorporation of ruthenium in the Pt/C nanowires and their decrease in metallic loading increased their efficiency towards the electrooxidation of methanol. The nanowires Pt_{0.6}Ru_{0.4}/C are thus promising materials as anodes for use in direct methanol fuel cells.

Keywords: nanowires; methanol electrooxidation; direct methanol fuel cell; Pt-Ru electrocatalysts.

1. INTRODUCTION

In a society where oil is the main source of energy, the great demand combined with a decreasing supply makes the price of this fuel fluctuate almost permanently, which is further impaired by the gases generated from the burning of this fuel. The concept of sustainable development widely discussed in recent years *versus* an exponential growth in energy demand, which is mostly supplied by fossil fuels, causes high amounts of pollutants to be released into the atmosphere due to the burning of these fuels directly contributing for global warming. Facing the current problem, several research groups around the world are developing new sources of energy capable of minimizing environmental pollution, thus minimizing the impact on future generations. In this context, hydrogen is a promising fuel that can be used in fuel cells [1]. However, it is known that the logistics of its use is a problem for commercialization and industrial application.

Among the alternative technologies being developed, direct alcohol fuel cells have become a highly interesting energy option, and one of the major challenges in using methanol (CH_3OH) as a fuel is to achieve high anodic catalytic performance of the alcohol oxidation reaction [2]. This kind of fuel cells is basically electrochemical devices that directly convert the chemical energy stored in the fuel into electricity and have several advantages such as: high efficiency (40-60%), easy operation and are considered environment friendly systems, despite its slow reaction kinetics in the oxidation of methanol [3].

Platinum has been used as a catalyst for direct methanol fuel cells (DMFCs), which are promising sources of energy for portable electronic devices and electric vehicles [4]. However, the cost and the lack of metal supply have hampered its commercial utilization. Another important point is that the formation of intermediate products, such as CO, during the oxidation reaction, significantly reduced the performance of this metal as anodic catalysts [5]. To solve this problem, the substitution of nanostructured materials from 0D to 1D, such as nanowires (NWs) [1,6], the insertion of several more active elements [7–9], the use of different support materials and the use of different catalysts synthesis method [10–13] have been investigated to improve catalytic activity towards methanol oxidation.

Electrochemical characteristics of the nanostructured electrode materials are strongly dependent on their grain size, texture, surface area and morphology [14,15]. In this sense, the ordered structure and high surface area of the nanowires can improve the electrochemical properties and the electrocatalytic activity of nanocatalysts [16]. In addition, they can improve the mass and electron transport due to their distinct morphology and structural properties [17], reducing the amount of electrocatalysts incorporated in the electrodes [18].

The Pt nanoelectrocatalysts associated with ruthenium has a high tolerance to CO, since Ru provides oxygenated species (OH_{ads}) at lower potentials than Pt, known as bifunctional mechanism [19,20]. On the other hand, the tolerance to CO in materials containing Pt–Ru can also be associated to the electronic effect that decreases the adsorption energy of the CO at the surface of the catalyst [21].

The atomic ratio of Pt–Ru has an important influence on the performance of the DMFCs catalysts, where the ratio 1:1 provides a greater activity considering the oxidation reactions of CO and methanol [22]. However, previous studies carried out in our group showed that the nanowires with the

60:40 (Pt:Ru) atomic ratio are more catalytic towards methanol oxidation than the other studied compositions (50:50, 70:30, 80:20 and 90:10) [23].

Different methodologies have been studied to synthesize Pt–Ru catalysts using a variety of reducing agents for metal precursors, such as sodium borohydride [24] and formic acid [25,26]. The utilization of surfactants during the synthesis process is generally used to prevent the agglomeration of the colloids during the metal precursors phase reduction [27]. To the best of knowledge, this paper is the first attempt to develop Pt–Ru nanowires by chemical reduction without the use of surfactants during the synthesis. In addition, the influence of different metallic loads of nanowires on the methanol oxidation activity is also unavailable in literature.

Therefore, in the present report, Pt and Pt–Ru nanowires supported on carbon powder have been developed varying the metal loading between 20, 30 and 40%. These materials are shown to be highly active for the electro-oxidation of methanol in acidic medium. The nanocatalysts were characterized by X-ray diffraction (XRD), X-ray fluorescence (XRF), transmission electron microscopy (TEM) and cyclic voltammetry. It was observed that the variation in the metallic loading of the precursor salts is a determining factor for the increase in the catalytic activity of the nanowires.

2. EXPERIMENTAL PROCEDURE

2.1. Pt and Pt–Ru nanowires preparation

The Pt/C and Pt_{0.6}Ru_{0.4}/C nanowires were synthesized according to the chemical reduction method [28–30]. The metal loading was varied, in the proportions of 40%, 30%, 20% relative to the carbon substrate (Vulcan[®]XC72). Formic acid (Sigma-Aldrich[®], 98-100% purity) was used as a reducing agent. All experiments were performed at room temperature in aqueous solution free of surfactants.

For the growth of the Pt and Pt–Ru metals on the carbon substrate, the synthesis was performed using hexachloroplatinic acid (Sigma-Aldrich[®], 37.5% Pt) and/or ruthenium chloride (Sigma-Aldrich[®], 45.55% Ru) dissolved in an aqueous solution. After the initial dispersion, an amount of carbon was added under stirring at 100 rpm for 30 minutes and finally the formic acid was inserted to reduce the metal ions onto the carbon substrate. The solution was then stored at room temperature for 72 hours. The synthesis product was filtered using a vacuum pump model PRISMATEC 131 and membrane in cellulose esters (with pores of 47 μm) from Millipore and the obtained powder was washed several times with ultrapure water for later drying at 60°C for 30 minutes in an oven. All aqueous solutions were prepared with ultrapure water obtained by a Gehaka model MS 2000 system.

2.2. Electrochemical Experiments

For the nanocatalyst fixation on the glassy carbon electrode of 5 mm in diameter, it was previously polished in 0.3 μm α-alumina suspension, then washed with ethanol and water in an ultrasonic bath to remove any alumina residues and finally dried at room temperature. For deposition of an ultrafine layer on the glassy carbon electrode, 0.0032 g of the synthesized composites was added

to 30 μL of a solution of 0.5% Nafion[®] (Aldrich[®], solution at 5% in aliphatic alcohols) and 1000 μL of isopropyl alcohol. This mixture was then subjected to an ultrasonic agitation (Ultrasonic QR500) for 30 minutes for complete homogenization. After this, 5 μL of this produced 'ink' was transferred to the electrode for complete coating of the glassy carbon and left at room temperature to dry.

Electrochemical measurements were performed on a potentiostat/galvanostat (Autolab model PGSTAT302N) coupled to a computer, operating with GPES Software version 4.9. The voltammetric profiles of the different electrocatalysts were obtained in a Pirex[®] glass one compartment electrochemical cell of, containing a reference electrode of hydrogen prepared in the same solution, a platinum counter electrode of 1 cm^2 and the glassy carbon electrode. As support electrolyte, a 0.5 mol L^{-1} H_2SO_4 solution was prepared with ultrapure water, and previously saturated with nitrogen (N_2). All measures were taken with a scanning speed of 20 mV s^{-1} . All potentials are referred to the reversible hydrogen electrode (RHE). The cyclic voltammetry methanol oxidation studies were carried out in 0.5 mol L^{-1} methanol solution in 0.5 mol L^{-1} H_2SO_4 , as well as the chronoamperometric curves applying a potentiostatic jump from 0.05 V to 0.60 V, maintaining the potential for 3600 s.

The CO stripping voltammograms were obtained after bubbling the CO gas in the electrochemical cell for 5 minutes applying 0.1 V followed by bubbling with N_2 to remove the dissolved CO. Two voltammograms were recorded between 0.05 and 1.0 V at 10 mV s^{-1} . The analyses were performed to evaluate the catalysts tolerance to CO, as well as for the calculation of the electrode electroactive area used to normalize the currents. Pt/C (10 wt% of Pt) from Alfa Aesar commercial electro-catalyst was used as reference material for comparison purposes in the methanol oxidation experiments.

2.3. Physical Characterization

TEM analyses were performed using an electronic microscope JEOL 2100 HTP JEM at 200 kV. The XRD analyses were performed using a diffractometer (PANalytical EMPYREAN), operating with Cu $\text{K}\alpha$ radiation ($\lambda = 0.15406$ nm) and maximum power of 1600 W, generated in 40 kV and 40 mA. The parameters used (range angles $2\theta = 20^\circ - 90^\circ$, with $\nu = 2^\circ \text{min}^{-1}$) were kept constant throughout the analysis. Analyzes of the XRD patterns were performed using Philips X'pertHighScore Plus. The Scherrer equation was used to calculate the mean crystallite size of the peak height (220) with $2\theta = 67.68^\circ$. The network parameters were obtained using Bragg's law. The Pt:Ru ratios of the prepared nanowires were determined from the deposited amounts of Pt and Ru by XRF analysis on a S4PIONNER by Bruker-AXS2010.

3. RESULTS

3.1 Physical characterization

The XRD patterns of the Pt/C and PtRu/C nanowires, in Figure 1, display a characteristic diffraction peak (002) at $2\theta \approx 24^\circ$ attributed to the diffraction of the carbon support used, with a hexagonal structure. The three Pt/C electrocatalysts (20, 30 and 40 wt%) exhibited Pt diffraction peaks

(111), (200), (220) and (311) (vertical dashed lines) at $2\theta = 39.87^\circ$, 46.13° , 67.30° and 81.10° , respectively, characteristic of Pt with face-centered cubic structure (JCPDS-004-802).

The peaks of the Pt–Ru nanocatalysts are similar to those of Pt/C, except that the 2θ values are slightly shifted to more positive values ($2\theta = 40.07^\circ$, 46.38° , 67.68° and 81.59°). The change is attributed to the contraction of the lattice parameter, when smaller size Ru atoms substitute larger atoms of Pt followed by the formation of Pt–Ru alloy [10,31]. Moreover, in the pattern of Pt_{0.6}Ru_{0.4}/C 40wt%, three peaks corresponding to Ru (JCPDS: 06-0663) at $2\theta = 27.35$, 34.68 and 54.0° appear, where the two last peaks were also observed by Kim *et al.* [10] for Pt–Ru nanowires synthesized by electrospinning method.

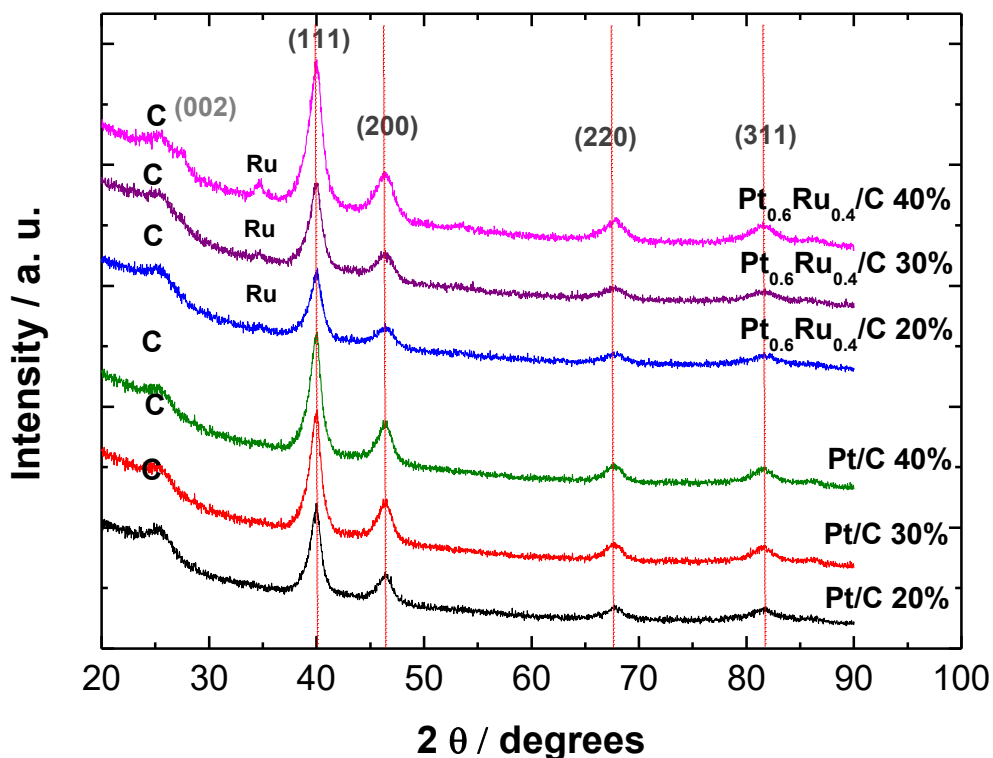


Figure 1. X-ray diffraction patterns obtained for the electrocatalysts prepared by the chemical reduction method. CuK α radiation with continuous scanning. Red dashed lines correspond to the position of the pure polycrystalline Pt peaks.

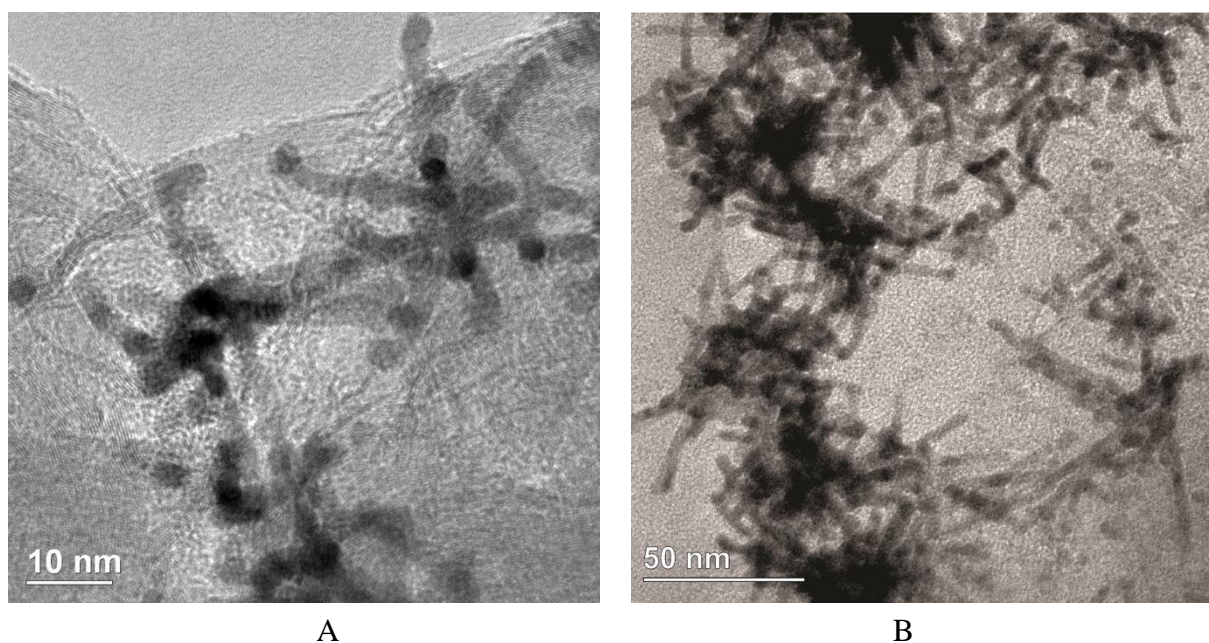
Lattice parameters values of Pt–Ru/C nanowire structures were calculated according to the Bragg's law using the diffraction peak (220) of Pt, which was not affected by the carbon support interaction. The values found were 0.3891, 0.3887 and 0.3879 nm for Pt_{0.6}Ru_{0.4}/C at 20, 30 and 40% respectively, compared to the lattice parameters of the platinum electrocatalysts (0.3914 nm) for 20% and 30% Pt/C and (0.3915 nm) for Pt/C 40%, the lattice parameter values of the Pt–Ru nanowires decreased with the compression of the Pt crystal lattice from the Ru insertion.

Table 1 contains the structural parameters of the mean crystallite size and the lattice parameter α determined for all developed catalysts. The average crystallite size ranged from 4.531, 4.874 and 4.566 nm for the Pt_{0.6}Ru_{0.4}/C nanowires with 20, 30 and 40%, respectively. Pt/C nanowires values varied from 5.2112, 5.3124 and 5.3224 nm for 20, 30 and 40%. For Calderón *et al.* [13] Pt–Ru nanocatalysts supported on carbon nanofibers, 20 wt% and 1:1 Pt–Ru atomic ratio, by impregnation and subsequent reduction by sodium borohydride or by the reduction method by formate ions and commercial Pt–Ru/C showed mean crystallite sizes of 4.0, 4.8 and 4.4 nm, respectively. The values presented by Calderón *et al.* [13] were close to the Pt_{0.6}Ru_{0.4}/C nanowires analyzed in this work; thus demonstrating a similar crystal grown by reduction.

Table 1. Structural parameters obtained by XRD and XRF techniques for electrocatalysts.

Electrocatalysts	Crystallite size (nm)	Lattice parameter (nm)	Pt–Ru ratio (at.%) (by XRF)
Pt/C 20%	5.2112	0.3914	-
Pt/C 30%	5.3124	0.3914	-
Pt/C 40%	5.3224	0.3915	-
Pt _{0.6} Ru _{0.4} /C 20%	4.531	0.3891	63.54:36.46
Pt _{0.6} Ru _{0.4} /C 30%	4.874	0.3887	61.26:38.74
Pt _{0.6} Ru _{0.4} /C 40%	4.566	0.3879	65.66:34.34

Furthermore, according to Table 1, the Pt–Ru ratios were quantified by XRF and presented results of 63.54:36.46, 61.26:38.74 and 65.66:34.34 for the Pt_{0.6}Ru_{0.4}/C 20%, 30% and 40% nanowires, respectively, close to nominal values. On the other hand, the representative TEM images of the Pt/C (40%) and the Pt_{0.6}Ru_{0.4}/C electrocatalysts with metal load of 20 and 40% are shown in Figure 2. Note that the method used in the preparation of the catalysts is efficient for the production of nanowires.



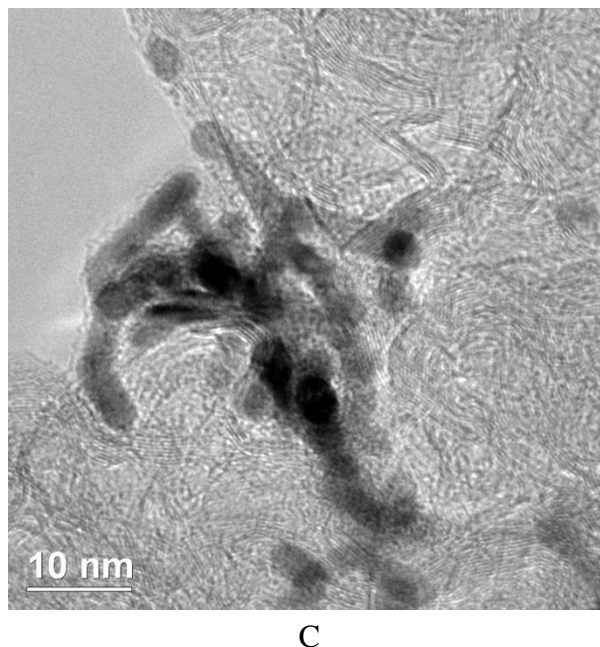


Figure 2. TEM micrographs of the nanowires Pt/C (A) (40%), Pt_{0.6}Ru_{0.4}/C (20%) (B) and Pt_{0.6}Ru_{0.4}/C (40%) determined by chemical reduction method.

The Pt/C nanowires (40%) had lengths and diameters of approximately 15 nm and 5 nm, and the Pt_{0.6}Ru_{0.4}/C (20% and 40%) 20 nm and 6 nm, as well as 13 nm and 4 nm, respectively. The Pt–Ru nanowires synthesized by Li *et al.* [30] by reduction with sodium borohydride in solution containing the cetyltrimethylammonium bromide surfactant presented a uniform distribution and diameter of 3 ± 0.5 nm. Whereas the nanowires synthesized in this work by chemical reduction and without surfactant presented diameters somewhat higher.

Zhang *et al.* [32] synthesized Pt nanowire matrices with diameters of 25 and 60 nm by electrodeposition from solution containing hexachloroplatinic and boric acid with anodic aluminum oxide as template. They also studied nanowires activities towards the oxygen reduction reaction in comparison with the Pt/C 20% commercial catalyst from Johnson Matthey. The current density of the commercial Pt/C was limited to around 0.09 mA/cm^2 , while for the nanowires of 60 and 25 nm it was 0.54 and 0.74 mA/cm^2 , which are 6 and 8 times higher, respectively, than the commercial catalyst. The improved activities of the Pt/C nanowires were attributed to their highly ordered structure which promoted increase in the electron and mass transfer rate. In addition, smaller diameter Pt/C nanowires exhibit better performance because the electrochemical surface area is higher.

Pt nanowires prepared by the electrodeposition method and further annealing at different temperatures (200, 400 and 600 °C) were studied for the oxygen reduction reaction (ORR) and methanol oxidation reaction (MOR) compared with commercial carbon supported catalysts [33]. All nanowires exhibited superior electrocatalytic activities for the two reactions. The activity of the MOR increased considerably with the increase of temperature while for the ORR the reverse happened. This phenomenon can be attributed to the rearrangement of the nanowires at the surface during the annealing. The nanowires were uniformly distributed with a length of approximately 10 nm. Since

more atoms are deposited when the deposition time is expanded, hence the length of the nanowires can be controlled by varying the time of electrochemical deposition.

According to Koenigsmann *et al.* [34] metallic ruthenium nanowires with further Pt deposition presented average diameters varying from 44 to 280 nm. The commercial Pt–Ru nanoparticles yielded mass activity of (0.61 A/mg of Pt) almost twice as higher than the Pt–Ru nanowires (0.36 A/mg Pt). Long-term durability tests demonstrated that due to the anisotropic nature of the Pt–Ru nanowires, it is less susceptible toward structural reconfiguration, while Pt–Ru nanoparticles suffered significant performance losses due to particle aggregation and ripening. With respect to methanol oxidation reaction, the Ru nanowires showed an improved catalytic activity compared to the Pt/C and Pt–Ru/C nanoparticles.

Scofield *et al.* [35] synthesized Pt–Ru–Fe nanowires by a solution technique based on the growth of the metal into a template consisting of a network of micelles with addition of a surfactant (hexadecyltrimethylammonium bromide) dissolved in chloroform. The nanowires presented an average diameter in the range of 1.9 to 2.2 nm.

Note that the nanowires developed in our study have a smaller wire diameter than the Ru nanowires with posterior Pt deposition [34], albeit are larger than the Pt–Ru–Fe trimetallic nanowires [35]. They are crystalline, in addition to being synthesized by a rapid and easily extended methodology by chemical reduction, at room temperature and surfactant free, presenting significant results towards methanol oxidation and representing a crucial step for the practical incorporation of 1D nanostructures.

3.2 Electrochemical Characterization

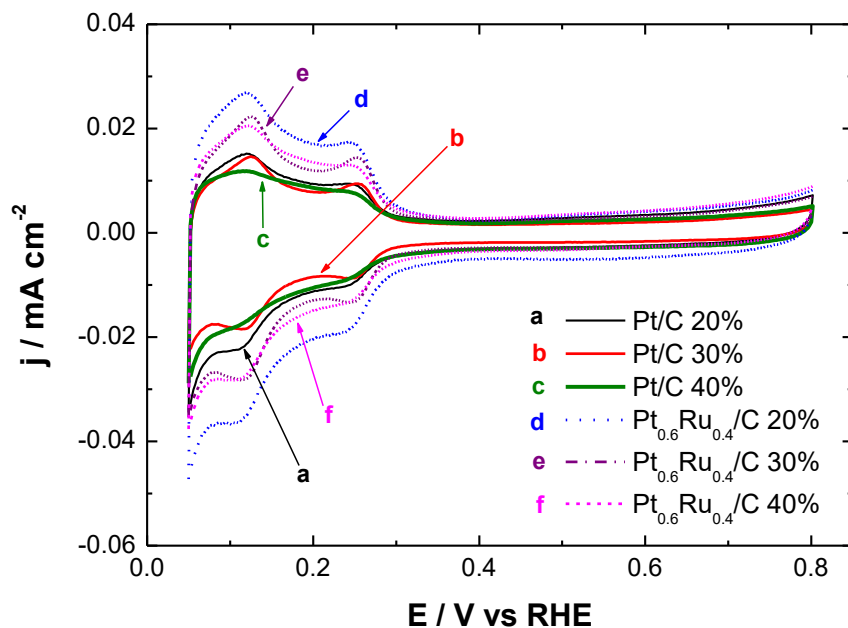
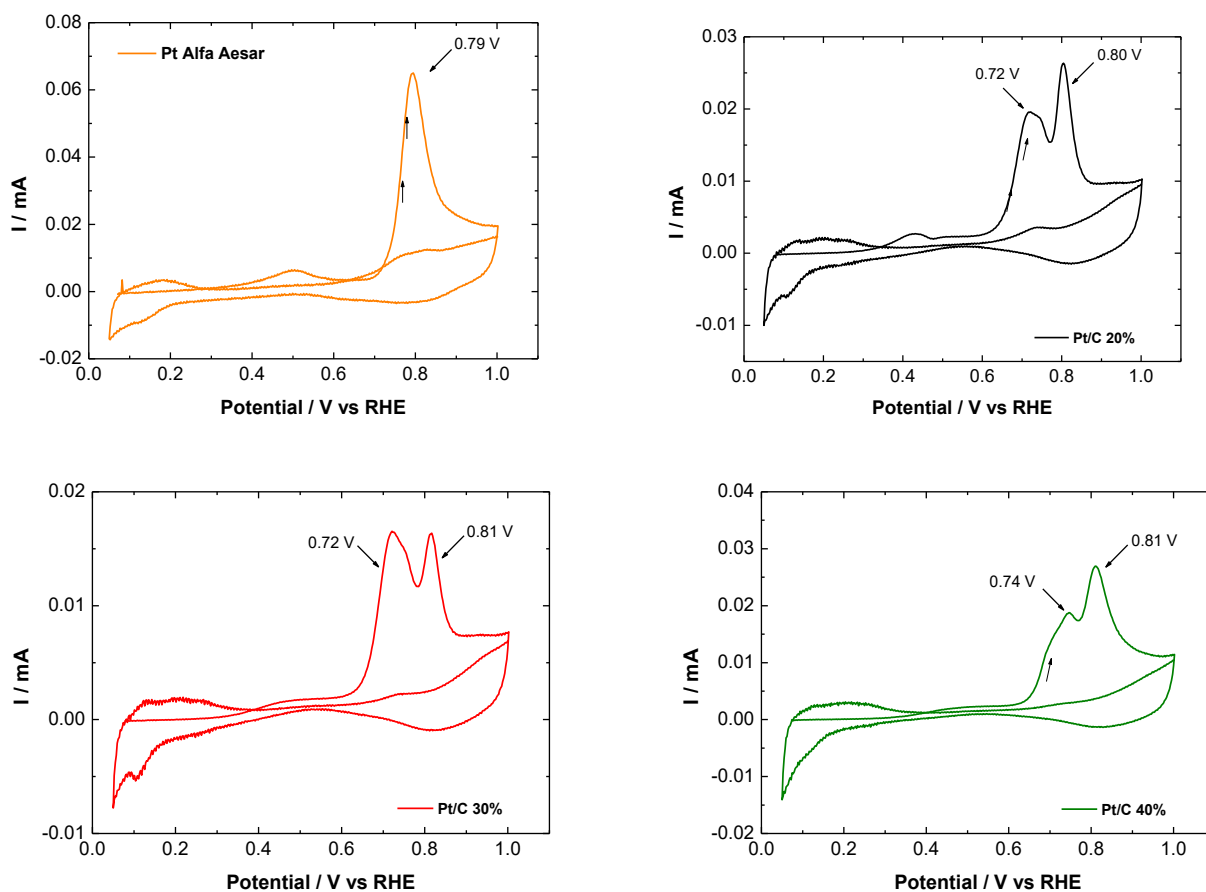


Figure 3. Cyclic voltammograms (second cycle) performed on the nanowires of: Pt/C 20%, Pt/C 30%, Pt/C 40%, Pt_{0.6}Ru_{0.4}/C 20%, Pt_{0.6}Ru_{0.4}/C 30%, Pt_{0.6}Ru_{0.4}/C 40% in the supporting electrolyte (0.5 mol L⁻¹ H₂SO₄) at $\nu = 20 \text{ mV s}^{-1}$.

The electrochemical characterization of the catalysts carried out in $0.5 \text{ mol L}^{-1} \text{ H}_2\text{SO}_4$ (Figure 3) showed that all catalysts exhibited hydrogen adsorption and desorption peaks between 0.05 and 0.30 V. This finding is consistent with previous reports of homogeneous alloys of Pt–Ru [34,35], demonstrating that polycrystalline Pt was deposited successfully on the nanowires synthesized by the chemical reduction method. In addition, the electric double layer loading region is wider for all the ruthenium-containing nanowires due to the presence of the alloy phase (Ru at the surface), and/or to the presence of ruthenium secreted (in metallic or oxide form) [34].

3.3 CO Stripping

The onset potential in the voltammograms of CO stripping is generally used to discern the CO tolerance of one nanocatalysts, in which, more negative potentials are related to higher CO tolerances. The area of the CO oxidation peak was also used to determine the electroactive area of the nanocatalysts, assuming a load of $420 \mu\text{C cm}^{-2}$ on the oxidation of a monolayer of CO adsorbed on the surface, Figure 4. The current densities in this work were calculated taking into account this electroactive area.



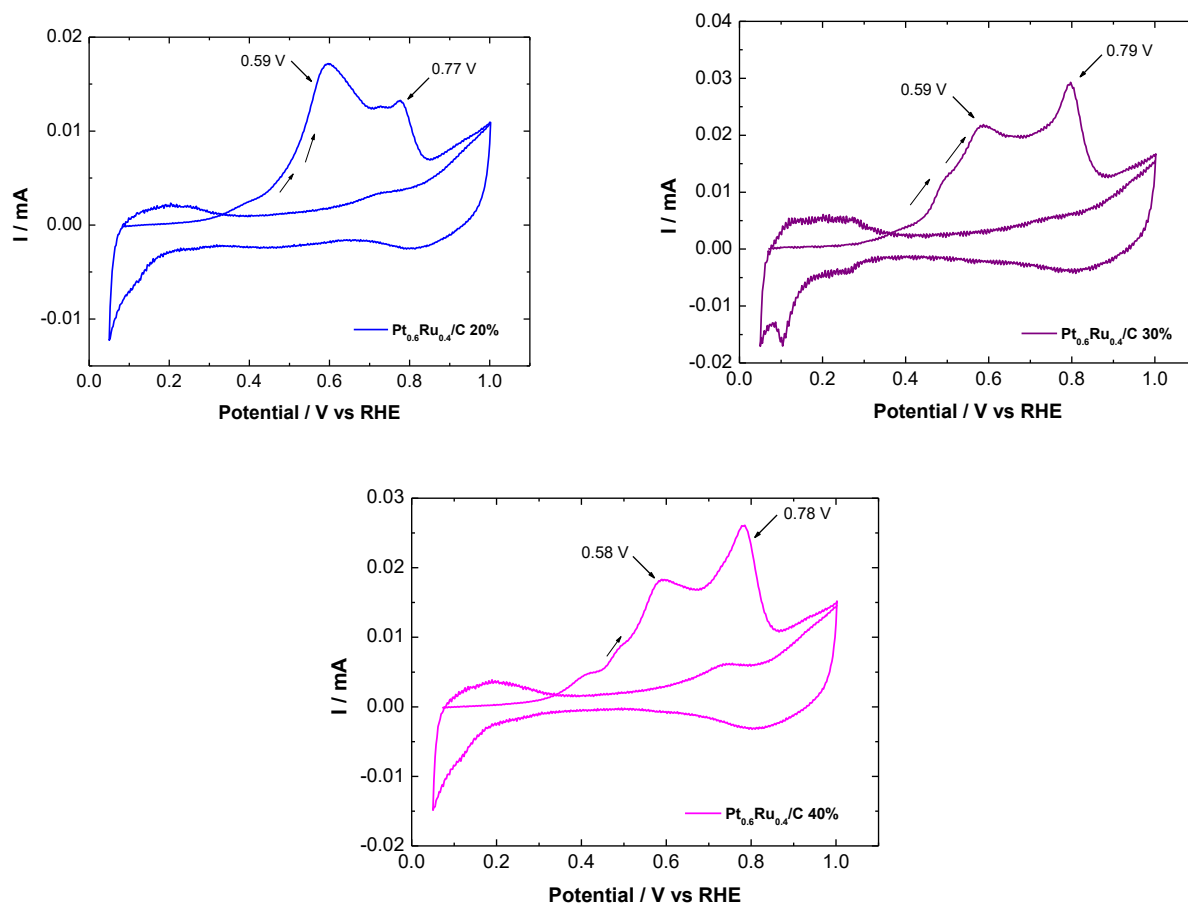


Figure 4. Cyclic voltammograms for CO oxidation on the electrodes: Pt/C Alfa Aesar, Pt/C 20%, Pt/C 30%, Pt/C 40%, Pt_{0.6}Ru_{0.4}/C 20%, Pt_{0.6}Ru_{0.4}/C 30% and Pt_{0.6}Ru_{0.4}/C 40% in acid medium (0.5 mol L⁻¹ H₂SO₄) at $v = 10 \text{ mV s}^{-1}$.

The onset of CO oxidation as well as the peak removal potential ($\approx 0.8 \text{ V}$) of the reference nanoparticles (Pt/C Alfa Aesar) agrees favorably with the literature data [36]. For Ru-containing nanowires, CO oxidation occurred at lower potentials when compared to commercial Pt and Pt nanowires. The Pt_{0.6}Ru_{0.4}/C 20% exhibited the lowest CO oxidation onset potential (0.34 V), while the location of the first oxidation peak was 0.59 V. The initial and peak oxidation potentials depend on the material and are presented in the following order: Pt_{0.6}Ru_{0.4}/C 20% (0.339 V) < Pt_{0.6}Ru_{0.4}/C 40% (0.359 V) < Pt_{0.6}Ru_{0.4}/C 30% (0.378 V) < Pt/C 20% (0.606 V) < Pt/C 30% (0.611 V) < Pt/C 40% (0.615 V) < Pt/C Alfa Aesar (0.725 V). Regarding the oxidation peak, it coincides partially with the onset of oxidation: Pt_{0.6}Ru_{0.4}/C 40% < Pt_{0.6}Ru_{0.4}/C 20% < Pt_{0.6}Ru_{0.4}/C 30% < Pt/C 20% < Pt/C 30% < Pt/C 40% < Pt/C Alfa Aesar. The differences observed in the voltammograms of CO removal to the Ru-containing could be associated to the surface motility of the CO adsorbed on the various crystalline faces [37]. In addition, increased CO tolerance by Ru insertion is regularly attributed to the bifunctional mechanism [19,20,38,39].

3.4 Methanol Electrochemical Oxidation

Methanol electrooxidation was studied by cyclic voltammetry in 0.5 mol L⁻¹ of methanol in 0.5 mol L⁻¹ H₂SO₄ (Figure 5). It is possible to observe an irreversible anode current during the direct scanning; being its value exceeded during the cathodic sweep and this can be associated to the intermediates in the surface of the electrocatalyst [40]. The adsorbed CO and CH_x species are formed during the anodic scanning. Hence, a lower stream is achieved compared to the cathodic sweep where the surface is almost free of adsorbed residues (at elevated potentials, the adsorbed methanolic fragments can oxidize) [19]. The electrooxidation of methanol started around 0.56 V for Pt_{0.6}Ru_{0.4}/C with 20 wt%, displacing about 0.10 V in the negative direction compared to Pt/C Alfa Aesar. It can be observed that the addition of Ru to the NW allowed a decrease in the oxidation initiation potential (all the onset potentials were obtained using a fixed value of $j = 0.02 \text{ mA cm}^{-2}$) in relation to the Pt/C and Pt/C Alfa Aesar (Table 2). For instance, it is worthwhile noticing that the onset potential of 0.56 V seen for Pt_{0.6}Ru_{0.4}/C with 20 wt% developed in this work is ~20 mV more negative than the seen for carbon supported PtRu core-shell catalysts using microwave-assisted method, followed by the in-situ reduction of Pt on Ru nanoparticles [41]. It is also ~40 mV more negative than the observed for Ru@Pt_{1.0}/C, Ru@Pt_{1.5}/C and ~10 mV than the Ru@Pt_{0.5}/C, catalyst, all synthesized by microwave-assisted method [42]. Further, onset potential seen for Pt_{0.6}Ru_{0.4}/C 20 wt% is ~10-20 mV lower than the ones taken for PtRu nanoparticles supported onto graphene and nitrogen-doped graphene [43]. Finally, the onset potential of the Pt_{0.6}Ru_{0.4}/C 20 catalyst is ~110 mV more negative than the one for a PtRu/C commercial catalyst (Johnson Matthey) [41]; thus demonstrating the role of the nanowire morphology in the catalyst performance, compared with state-of-the-art catalysts recently developed.

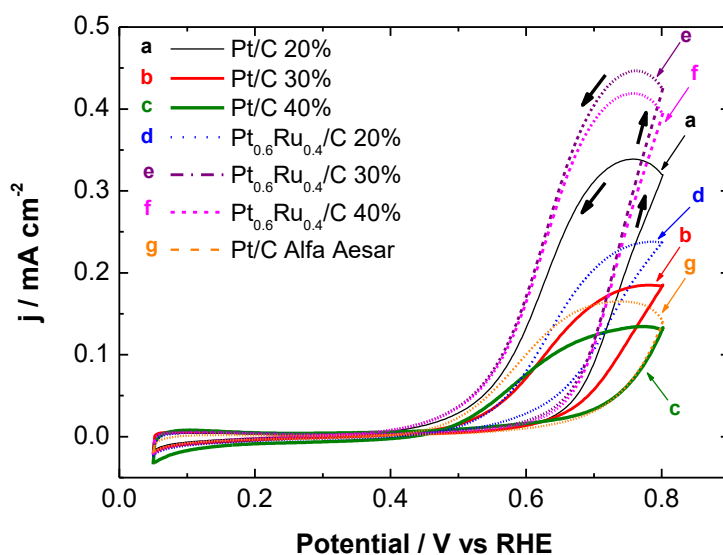


Figure 5. Cyclic voltammograms (second cycle) of the electrochemical oxidation of methanol (0.5 mol L⁻¹) on the nanowires-based electrodes: (a) Pt/C 20%, (b) Pt/C 30%, (c) Pt/C 40%, (d) Pt_{0.6}Ru_{0.4}/C 20%, (e) Pt_{0.6}Ru_{0.4}/C 30%, (f) Pt_{0.6}Ru_{0.4}/C 40% as well as (g) Pt/C Alfa Aesar in acid medium (0.5 mol L⁻¹ H₂SO₄) at $v = 20 \text{ mV s}^{-1}$.

Table 2. Onset potentials and methanol oxidation current peaks taken for all synthesized electrocatalysts.

Catalyst	$E_{\text{onset}} / \text{V}$	* $j / \text{mA cm}^{-2}$
Pt/C 20%	0.63	0.31
Pt/C 30%	0.63	0.18
Pt/C 40%	0.64	0.13
Pt _{0.6} Ru _{0.4} /C 20%	0.56	0.23
Pt _{0.6} Ru _{0.4} /C 30%	0.60	0.42
Pt _{0.6} Ru _{0.4} /C 40%	0.61	0.39
Pt/C Alfa Aesar	0.66	0.14

* Current density measured at 0.8 V *vs* RHE.

3.5 Chronoamperometry

The catalytic activity of the nanoelectrocatalysts was studied by measuring the current as a function of time using chronoamperometry and applying a potential of 0.6 V *versus* RHE for 1800 s in acid medium (0.5 mol L⁻¹ H₂SO₄) and 0.5 mol L⁻¹ methanol. Figure 6 shows the chronoamperometric curves normalized by the electroactive area.

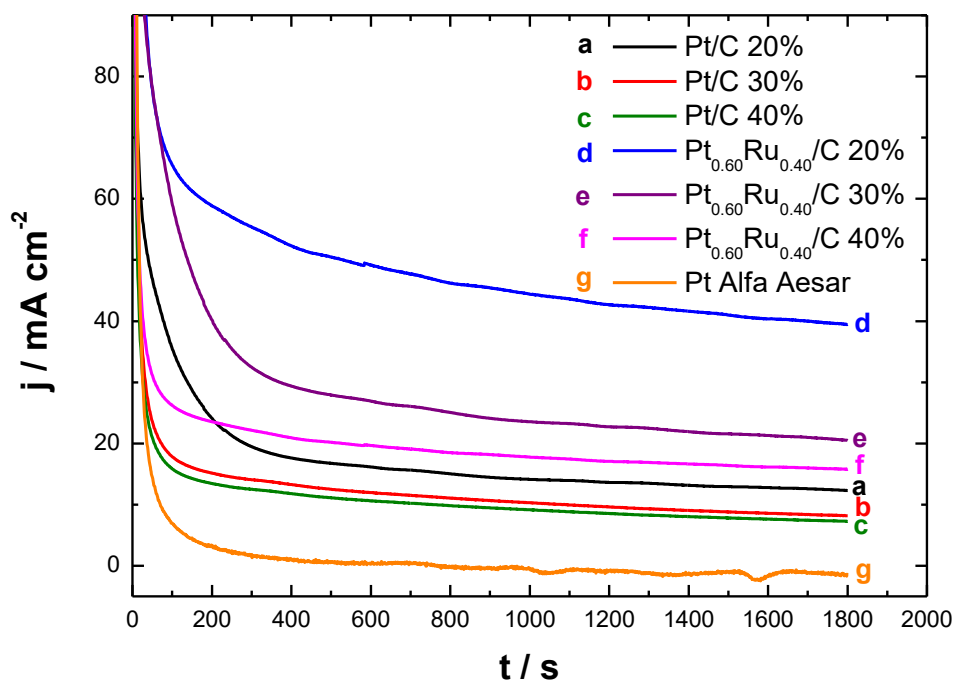


Figure 6. Chronoamperometric curves made in 0.5 mol L⁻¹ methanol solutions in 0.5 mol L⁻¹ H₂SO₄ taken by applying an anodic potential of 0.6 V during 1800 s on the nanowires Pt/C 20%, Pt/C 30%, Pt/C 40%, Pt_{0.6}Ru_{0.4}/C 20%, Pt_{0.6}Ru_{0.4}/C 30%, Pt_{0.6}Ru_{0.4}/C 40%, as well as commercial Pt/C.

After applying 0.6 V the capacitive current decays rapidly due to the double layer loading and other processes on the surface of the electrode. At the end of the 1800 s experiment, the Pt_{0.6}Ru_{0.4}/C

20% nanowires showed a high current density $j = 39.57 \text{ mA cm}^{-2}$ compared to Pt/C Alfa Aesar with $j = -1.47 \text{ mA cm}^{-2}$. This catalyst obtained a pseudo-current density twenty-six times greater compared to Pt/C Alfa Aesar. This increased catalytic activity may be due to the modified bifunctional mechanism when the water molecule required for complete methanol oxidation originates from the Ru surface. The Pt/C 20%, Pt/C 30%, Pt/C 40%, Pt_{0.6}Ru_{0.4}/C 30% and Pt_{0.6}Ru_{0.4}/C 40% nanowires at the end of the experiment presented current density values of about 12.29, 8.59, 7.12, 20.71 and 15.95 mA cm⁻², respectively.

The performance of the developed PtRu nanowire catalysts is higher than the reported for undoped nanodiamond supported Pt-Ru catalysts, in which a current density decays rapidly in the initial period because the electrocatalysts were poisoned due to the formation and gradual accumulation of intermediates such as CO_{ads}, CH₃OH_{ads} and CHO_{ads} on the surface of the catalyst during a methanol oxidation reaction preventing further reactions at active sites [44]. Similarly, the current density observed for the Pt_{0.6}Ru_{0.4}/C 20% nanowires (39.57 mA cm⁻²) is almost 500-fold higher than the observed for unsupported RuPt nanowire networks (Ru₅₆Pt₄₄) after 1800 s applying 0.6 V in 1.0 mol L⁻¹ methanol in 0.5 mol L⁻¹ H₂SO₄ [45].

For a better comparison of the catalytic performance of the nanocatalysts synthesized in this work, polarization curves were performed in a quasi-stationary state. These curves are used for the study of the electrochemical oxidation of methanol, since these provide a direct comparison between electrochemical activity of the nanocatalysts and initial oxidation potentials, meanwhile only the faradaic currents are considered to diminish the contribution of the capacitive processes.

3.6 Polarization Curves

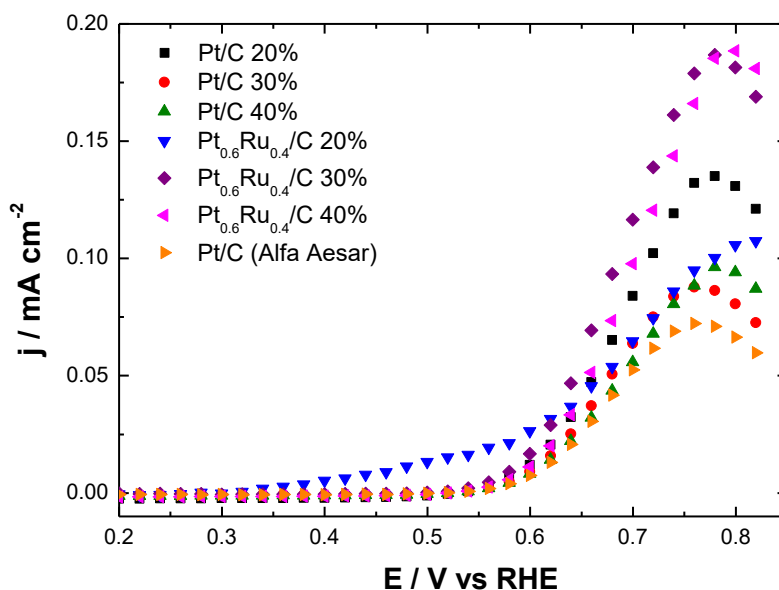


Figure 7. Polarization curves in stationary state for electrochemical oxidation of 0.5 mol L⁻¹ methanol in 0.5 mol L⁻¹ H₂SO₄ obtained on nanowires: Pt/C 20%, Pt/C 30%, Pt/C 40%, Pt_{0.6}Ru_{0.4}/C 20%, Pt_{0.6}Ru_{0.4}/C 30% and Pt_{0.6}Ru_{0.4}/C 40%.

Figure 7 shows the comparison between the polarization curves of the Pt/C and Pt–Ru/C nanowires with different metal loads. The data were obtained in potentiostatic mode after 300 s of polarization at each potential. The electrocatalytic activity improved for the oxidation of methanol on the nanowires Pt_{0.6}Ru_{0.4}/C with 20% metallic load.

The polarization curves indicate that the methanol oxidation process starts at 0.59; 0.60; 0.61; 0.47; 0.58; 0.59; 0.61 V *versus* RHE on the Pt/C, Pt_{0.6}Ru_{0.4}/C nanowires with 20, 30 and 40% metallic load and Pt/C Alfa Aesar, respectively, as shown in Table 3. Values of methanol oxidation onset potential were measured at 0.01 mA cm⁻². The table shows that the nanowires Pt_{0.6}Ru_{0.4}/C with 20% of metallic load presented a decrease in the beginning of the oxidation reaction of methanol in 0.12, 0.13 and 0.14 V when compared with Pt/C 20, 30, 40% and commercial Pt, respectively. The Pt_{0.6}Ru_{0.4}/C nanowires with 30 and 40% of metallic load presented the oxidation reaction onset in more positive potentials (approximately 0.11 and 0.12 V *versus* RHE) in comparison to the Pt_{0.6}Ru_{0.4}/C nanowires with 20% metal load. The addition of ruthenium to the electrocatalyst produces a very active material, reducing the initial reaction potential for nanowires. The current density values determined at 0.6 V are also shown in Table 3.

Table 3. Parameters obtained in the polarization curves of Figure 7: Onset potential of the electrochemical oxidation of methanol and current pseudo-density for the electrocatalysts.

Nanowire	Onset potential of reaction <i>versus</i> RHE	Current density (mA cm ⁻²) determined at 0.6 V
Pt/C 20%	0.59	0.012
Pt/C 30%	0.60	0.008
Pt/C 40%	0.61	0.008
Pt _{0.6} Ru _{0.4} /C 20%	0.47	0.025
Pt _{0.6} Ru _{0.4} /C 30%	0.58	0.016
Pt _{0.6} Ru _{0.4} /C 40%	0.59	0.012
Pt/C Alfa Aesar	0.61	0.008

The nanowires Pt_{0.6}Ru_{0.4}/C with 20% metal loading showed a current density ~3.2 times higher than the observed for Pt/C Alfa Aesar; whereas Pt_{0.6}Ru_{0.4}/C nanowires with 30 and 40% metal loading the increase in current density was ~2 and 1.5 times, respectively. However, carbon oxidation in potential fuel cell operations limits long-term stability of the supported catalysts on carbon [46]. In this context, if the catalyst particles do not retain their structure over the life of the cell, the change in the morphology of the catalyst may result in the loss of the electrochemical activity of the catalyst [47] that is more difficult for nanowires.

4. CONCLUSIONS

The chemical reduction method used in the synthesis process of the Pt/C and Pt_{0.6}Ru_{0.4}/C nanowires using formic acid as a reducing agent proved to be efficient for the formation of Pt/C and Pt_{0.6}Ru_{0.4}/C nanowires at different loads. According to the electrochemical analyzes, methanol

oxidation in ruthenium-containing nanowires occurred at lower values than the Pt/C nanowires; in addition, it can be observed that the catalyst with a lower deposited metallic loading was the one with the highest performance for the electrooxidation of methanol.

Crystalline Pt was successfully reduced in both Pt/C and Pt_{0.6}Ru_{0.4}/C nanowires, indicating the formation of both PtRu alloy and Ru islands for nanowires containing ruthenium in its composition. The nanowires yield better catalytic activity towards the electrooxidation of methanol. The values of current density found in the electrochemical studies for the electrooxidation of methanol in acid medium are higher for the ruthenium-containing electrocatalysts, indicating that the kinetic of reaction is faster. The results found in the CO removal studies indicated that addition of a second metal (Ru) to the Pt/C nanowire synthesis process increased the tolerance for the poisoning of synthesized nanocatalysts. Pt–Ru/C nanowires proved to be highly active electrocatalytic materials for the oxidation of methanol using a fairly simple set-up methodology that could be used as anodes in DMFCs.

ACKNOWLEDGEMENTS

The authors thanks to CNPq (grants: 303630/2012-4, 474261/2013-1, 407274/2013-8, 402243/2012-9, 400443/2013-9 and 310282/2013-6), to CAPES and to FAPITEC for the scholarships and financial support for this work.

References

1. L. Zhu, Q. Cai, F. Liao, M. Sheng, B. Wu and M. Shao, *Electrochem. Commun.*, 52 (2015) 29.
2. F. J. R. Varela, A. A. G. Coronado, J. C. Loyola, Q.-Z. Jiang and P. B. Perez, *J. New Mat. Electrochem. Syst.*, 14 (2011) 75.
3. J. M. Andújar and F. Segura, *Renew. Sust. Energ. Rev.*, 13 (2009) 2309.
4. C. K. Dyer, *J. Power Sources*, 106 (2002) 31.
5. R. Kannan, K. Karunakaran and S. Vasanthkumar, *J. New Mat. Electrochem. Syst.*, 15 (2012) 249.
6. Y. Lu, S. Du and R. Steinberger-Wilckens, *Appl. Catal. B – Environ.*, 164 (2015) 389.
7. K. I. B. Eguiluz, G. R. P. Malpass, M. M. S. Pupo, G. R. Salazar-Banda and L. A. Avaca, *Energy & Fuels*, 24 (2010) 4012.
8. H.-Y. Chou, C.-K. Hsieh, M.-C. Tsai, Y.-H. Wei, T.-K. Yeh and C.-H. Tsai, *Thin Solid Films*, 584 (2015) 98.
9. G. R. Salazar-Banda, K. I. B. Eguiluz, M. M. S. Pupo, H. B. Suffredini, M. L. Calegaro and L. A. Avaca, *J. Electroanal. Chem.*, 668 (2012) 13.
10. Y. S. Kim, S. H. Nama, H.-S. Shim, H.-J. Ahn, M. Anand and W. B. Kim, *Electrochem. Commun.*, 10 (2008) 1016.
11. C. Li, V. Malgras, S. M. Alshehri, J. H. Kim and Y. Yamauchi, *Electrochim. Acta*, 183 (2015) 107.
12. K. I. B. Eguiluz, G. R. Salazar-Banda, D. Miwa, S. A. S. Machado and L. A. Avaca, *J. Power Sources*, 179 (2008) 42.
13. J. C. Calderón, G. García, L. Calvillo, J. L. Rodríguez, M. J. Lázaro and E. Pastor, *Appl. Catal. B – Environ.*, 165 (2015) 676.
14. S.-B. Han, Y.-J. Song, J.-M. Lee, J.-Y. Kim and K.-W. Park, *Electrochem. Commun.*, 10 (2008) 1044.
15. M.-C. Tsai, T.-K. Yeh and C.-H. Tsai, *Electrochem. Commun.*, 8 (2006) 1445.
16. W. C. Choi and S. I. Woo, *J. Power Sources*, 124 (2003) 420.
17. S. Sun, G. Zhang, D. Geng, Y. Chen, R. Li, M. Cai and X. Sun, *Angew. Chem. Int. Ed.*, 50 (2011)

- 422.
18. S. M. Choi, J. H. Kim, J. Y. Jung, E. Y. Yoon and W. B. Kim, *Electrochim. Acta*, 53 (2008) 5804.
 19. S. Motoo and T. Okada, *J. Electroanal. Chem.*, 157 (1983) 139.
 20. M. Watanabe, M. Shibata and S. Motoo, *J. Electroanal. Chem.*, 187 (1985) 161.
 21. F. B. Mongeot, M. Scherer, M. Gleich, E. Kopatzki and R. J. Behm, *Surf. Sci.*, 411 (1998) 249.
 22. J. C. Calderón, G. García, A. Querejeta, F. Alcaide, L. Calvillo, M. J. Lázaro, J. L. Rodríguez and E. Pastor, *Electrochim. Acta*, 186 (2015) 359.
 23. G. R. O. Almeida, L. S. R. Silva, G. F. Pereira, A. Bueno-López, F. E. López-Suárez, K. I. B. Eguiluz and G. R. Salazar-Banda, *J. Solid State Electrochem.*, submitted.
 24. M. Harada and H. Einaga, *J. Colloid Interface Sci.*, 308 (2007) 568.
 25. J. R. C. Salgado, J. C. S. Fernandes, A. M. B. Rego, A. M. Ferraria, R. G. Duarte and M. G. S. Ferreira, *Electrochim. Acta*, 56 (2011) 8509.
 26. J. R. C. Salgado, V. A. Paganin, E. R. Gonzalez, M. F. Montemor, I. Tacchini, A. Ansón, M. A. Salvador, P. Ferreira, F. M. L. Figueiredo and M. G. S. Ferreira, *Int. J. Hydrogen Energy*, 38 (2013) 910.
 27. X. Wang and I-M. Hsing, *Electrochim. Acta*, 47 (2002) 2981.
 28. S. H. Sun, D. Q. Yang, G. X. Zhang, E. Sacher and J. P. Dodelet, *Chem. Mater.*, 19 (2007) 6376.
 29. S. Sun, G. Zhang, D. Geng, Y. Chen, R. Li, M. Cai and X. Sun, *Angew. Chem. Int. Ed.*, 50 (2011) 422.
 30. B. Li, D. C. Higgins, S. Zhu, H. Li, H. Wang, J. Ma and Z. Chen, *Catal. Commun.*, 18 (2012) 51.
 31. A. L. Ocampo, M. Miranda-Hernández, J. Morgado, J. A. Montoya and P. J. Sebastian, *J. Power Sources*, 160 (2006) 915.
 32. M. Zhang, J.-J. Li, M. Pan and D.-S. Xu, *Acta Physico-Chimica Sinica*, 27 (2011) 1685.
 33. Y. Su, M. Feng, C. Zhang, Z. Yan, H. Liu, J. Tang and H. Du, *Electrochim. Acta*, 164 (2015) 182.
 34. C. Koenigsmann, D. B. Semple, E. Sutter, S. E. Tobierre and S. S. Wong, *Appl. Mater. Interfaces*, 5 (2013) 5518.
 35. M. E. Scofield, C. Koenigsmann, L. Wang, H. Liu and S. S. Wong, *Energy Environ. Sci.*, 8 (2014) 350.
 36. H. A. Gasteiger, N. M. Markovic, P. N. Ross and E. J. Cairns, *J. Phys. Chem.*, 98 (1994) 617.
 37. F. Maillard, M. Eikerling, O. V. Cherstiouk, S. Schreier, E. Savinova and U. Stimming, *Faraday Discuss.*, 125 (2004) 357.
 38. M. Watanabe and S. Motoo, *J. Electroanal. Chem.*, 60 (1975) 267.
 39. A. A. Siller-Ceniceros, M. E. Sánchez-Castro, D. Morales-Acosta, J. R. Torres-Lubian, E. Martínez G., F.J. Rodríguez-Varela, *Appl. Catal. B-Environ.*, 209 (2017) 455.
 40. O. Guillén-Villafuerte, G. García, R. Guil-López, E. Nieto, J. L. Rodríguez, J. L. G. Fierro and E. Pastor, *J. Power Sources*, 231 (2013) 163.
 41. Y. Hu, A. Zhu, Q. Zhang and Q. Liu, *Int. J. Hydrogen Energy*, 41 (2016) 11359.
 42. J. Xie, Q. Zhang, L. Gu, S. Xu, P. Wang, J. Liu, Y. Ding, Y. F. Yao, C. Nan, M. Zhao, Y. You and Z. Zou, *Nano Energy*, 21 (2016) 247.
 43. Z. Yang, S. Xu, J. Xie, J. Liu, J. Tian, P. Wang and Z. Zou, *J. Appl. Electrochem.*, 46 (2016) 895.
 44. Y. Zhang, Y. Wang, L. Bian, R. Lu and J. Zang, *Int. J. Hydrogen Energy*, 41 (2016) 4624.
 45. W. Zhao, D. Huang, Q. Yuan and X. Wang, *Nano Res.*, 9 (2016) 3066.
 46. K.-W. Park, Y.-W. Lee, J.-K. Oh, D.-Y. Kim, S.-B. Han, A.-R. Ko, S.-J. Kim and H.-S. Kim, *J. Ind. Eng. Chem.*, 17 (2011) 696.
 47. E. Antolini, *Appl. Catal. B-Environ.*, 88 (2009) 1.